Science Advances
AAAS

advances.sciencemag.org/cgi/content/full/6/19/eaba1951/DC1

Supplementary Materials for

The lightness of water vapor helps to stabilize tropical climate

Seth D. Seidel and Da Yang*

*Corresponding author. Email: dayang@ucdavis.edu

Published 6 May 2020, *Sci. Adv.* **6**, eaba1951 (2020)
DOI: 10.1126/sciadv.aba1951

This PDF file includes:

Supplemental Text

S1. Clouds and All-Sky Radiation

The focus of this paper is to understand a clear-sky feedback. Therefore, the main text only uses the "clear-sky" model output radiation. The reader may naturally wonder whether a negative climate feedback is still observed in all-sky radiation, and we present those data here. For all-sky fluxes, Outgoing Shortwave Radiation (OSR) and Outgoing Longwave Radiation (OLR) are defined as:

$$OSR^{all} = F_{SW}^{\uparrow} - F_{SW}^{\downarrow} \quad [S1]$$

$$OLR^{all} = F_{LW}^{\uparrow} - F_{LW}^{\downarrow} \quad [S2]$$

$F_{SW}^{\uparrow}$ and $F_{SW}^{\downarrow}$ are the upwelling and downwelling shortwave fluxes at the top of the atmosphere (TOA). $F_{LW}^{\uparrow}$ and $F_{LW}^{\downarrow}$ are the upwelling and downwelling longwave fluxes at TOA. As in the body of the paper, we define OLR and OSR such that a positive value indicates a net upward flux. OSR^{all} should have a negative value. All of these values include the effect of clouds on radiation.

We are then able to define values of ΔOSR^{all} and ΔOLR^{all} which capture the all-sky radiative effects of vapor buoyancy. These are calculated as the domain-averaged differences between the control and mechanism-denial simulations:

$$\Delta OSR^{all} = OSR_{v}^{all} - OSR_{nv}^{all} \quad [S3]$$

$$\Delta OLR^{all} = OLR_{v}^{all} - OLR_{nv}^{all} \quad [S4]$$

Once again, the subscripts *v* and *nv* indicate control and mechanism-denial atmospheres, respectively. ΔOSR^{all} and ΔOLR^{all} are presented in Fig. S1a. ΔOLR^{all} closely follows ΔOLR^{clr}, and ΔOSR^{all} also shows qualitatively similar trends. Figure S1b shows the shortwave

and longwave cloud radiative effects due to vapor buoyancy. These are calculated by subtracting the clear-sky radiative effect from the all-sky radiative effect:

$$\Delta OSR^{cld} = \Delta OSR^{all} - \Delta OSR^{clr} \quad [S5]$$

$$\Delta OLR^{cld} = \Delta OLR^{all} - \Delta OLR^{clr} \quad [S6]$$

The change in net cloud radiative effect, ΔCRE_{net}, is the sum of the separate shortwave and longwave cloud effects:

$$\Delta CRE_{net} = \Delta OSR^{cld} + \Delta OLR^{cld}. \quad [S7]$$

We find that ΔCRE_{net} and its variation are dominated by the shortwave component (Fig. S1b). The longwave component varies little with SST. To illustrate how these cloud effects arise, we show plots of cloud fraction for five simulation pairs (Fig. S2). The control simulations (with vapor buoyancy) tend to have greater cloud amount than the mechanism-denial simulations. However, this difference lies almost entirely in the lower troposphere. There, the longwave effect is relatively weak, but the shortwave effect is strong. This might explain the dominance of ΔOSR^{cld} in our calculation of the net cloud radiative effect ΔCRE_{net}.

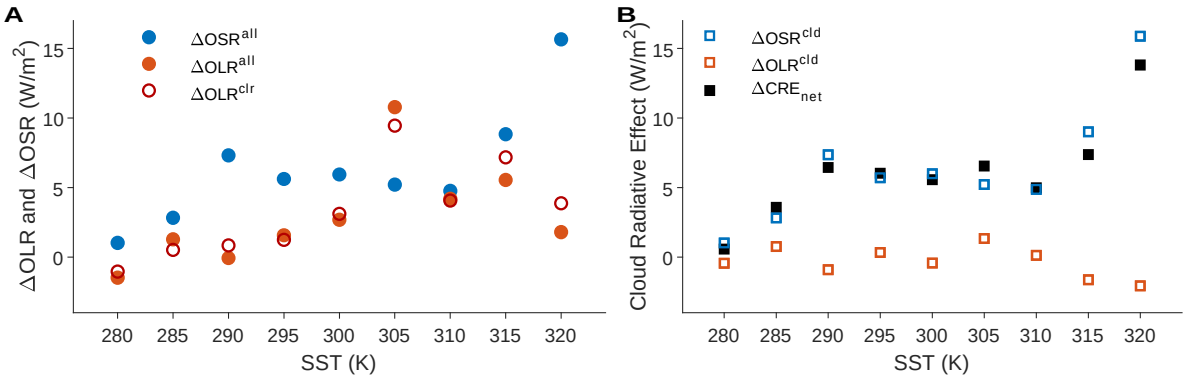

Figure S1. **All-sky and cloud effects on radiation. (A)** The all-sky shortwave and longwave radiative effects of vapor buoyancy. Clear-sky ΔOLR, from Fig. 5A, is presented for comparison to all-sky ΔOLR. **(B)** The cloud radiative effects due to adding vapor buoyancy.

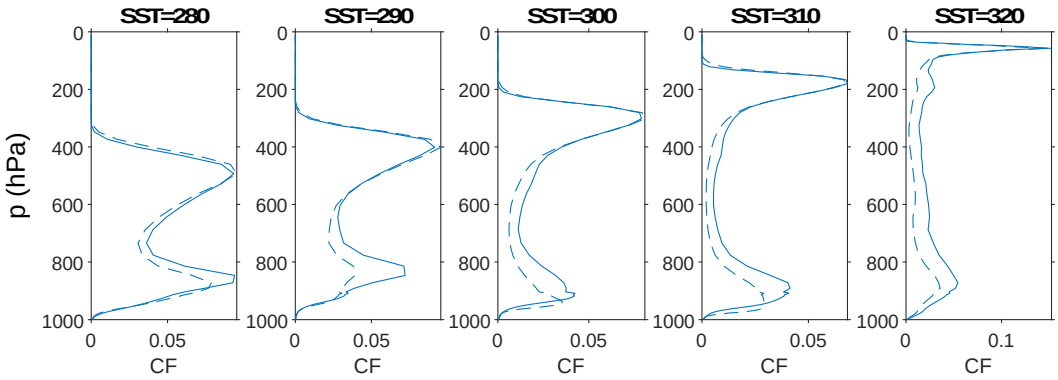

Figure S2. Time-averaged cloud fraction. These plots show how much of the simulation domain is occupied by clouds. Solid line: control simulations, with the vapor buoyancy effect turned on. Dashed line: mechanism-denial simulations, with the vapor buoyancy effect turned off.

S2. Radiative Kernels

Figure S3 presents the radiative kernel calculations discussed in the Methods section. The first two columns represent the kernels as actually applied in this study. The third column is what the water vapor kernel looks like under an assumption of constant relative humidity with climate warming. We do not apply this assumption, and we present this kernel only so that a reader may confirm that it is similar to past work on radiative kernels.

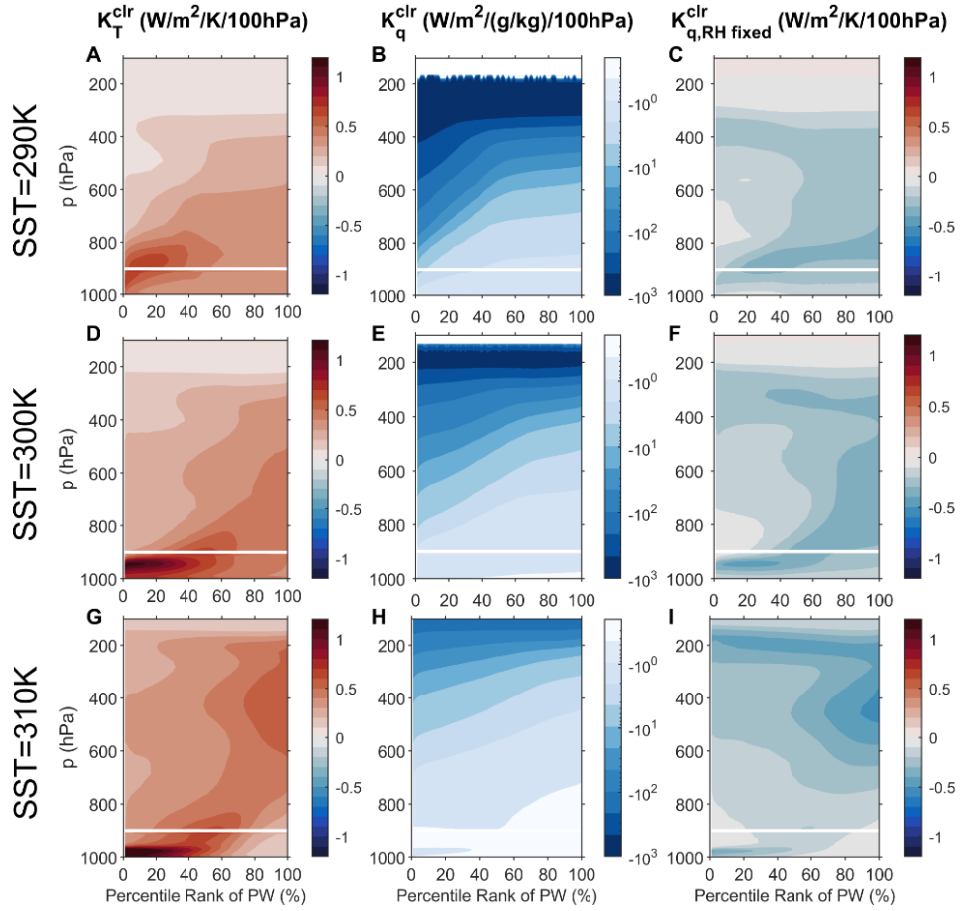

Figure S3. Radiative kernels. (A, D, G) The temperature radiative kernel, which reflects the sensitivity of clear-sky OLR to changes in atmospheric temperature. **(B, E, H)** The specific humidity radiative kernel, which reflects the sensitivity of clear-sky OLR to changes in atmospheric water vapor. We do not show values where they become positive in the stratosphere. **(C, F, I)** The specific humidity radiative kernel applied to increased water vapor from warming at constant-relative humidity. The white lines denote the 900 hPa level we use for the boundary layer top.

S3. Tropopause Identification

As discussed in the main text, we identify tropopause where time- and domain-averaged radiative heating becomes approximately zero in the control simulations. Figure S4 shows the radiative cooling profiles for our simulations. Figure S5 shows the identified tropopause level, which becomes higher with increasing surface temperature. For the SST = 320 K simulation, radiative cooling rate switches sign in the boundary layer. We ignored those levels when identifying the tropopause.

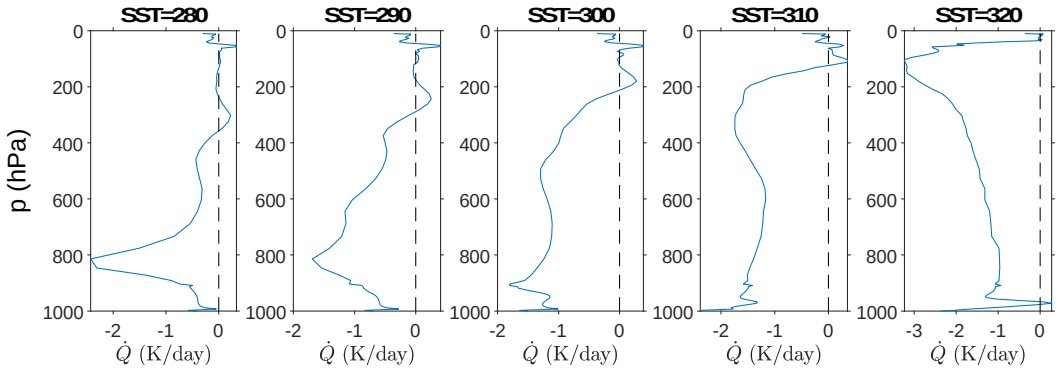

Figure S4. Radiative heating profiles. The time- and domain-averaged radiative heating rate profiles for several surface temperatures. These are derived from the control simulations.

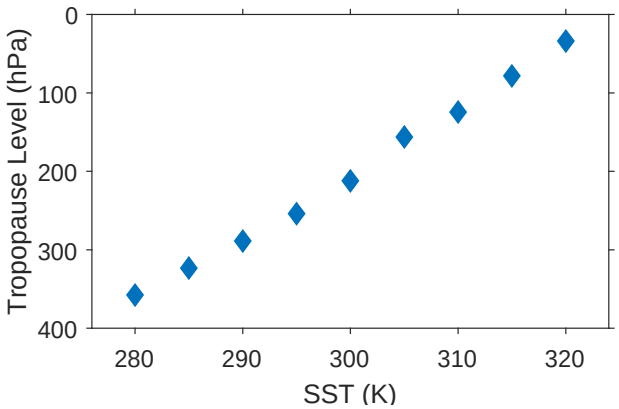

Figure S5. **Tropopause level.** The radiative tropopause level identified for each SST.

S4. Alternative Boundary Layer Top

We have used 900 hPa as the boundary layer top in the main text of this paper. Here, we perform a sensitivity analysis on the choice of the boundary layer top. We have considered the effect of an alternative boundary layer top, at $p = 800$ hPa. In Fig. S6, we decompose ΔOLR using this new boundary layer top. The overall magnitude and trend of the estimated radiative effect are preserved. Our results are robust to this alternative.

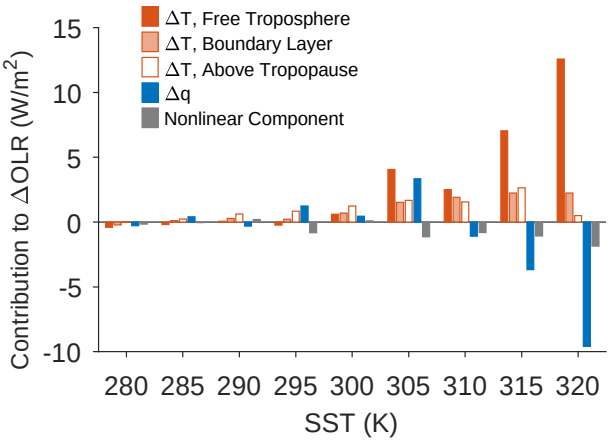

Figure S6. Decomposition of ΔOLR using an alternative boundary layer top. The same as Fig. 5b, except considering 800 hPa as the boundary layer top: Domain-averaged ΔOLR decomposed into components due to the linear effects of both temperature and water vapor. Tropopause was identified as the lowest level where domain- and time-averaged radiative heating is approximately zero in the simulation with vapor buoyancy. The nonlinear component is calculated as the residual of the ΔOLR from the simulations.

S5. Alternative Calculation of ΔT

In our theoretical calculation of ΔT, we used data only from the control simulation (rather than the simulation pairs) by comparing each column's temperature to that of a saturated, convecting column. While Fig. 6 in the main text is convincing, we present here an alternative calculation meant to further validate Fig. 6. Here we calculate ΔT by using the moisture profile of the most humid columns, which on average is not saturated. This is accomplished by modifying equation [4] from the main text. We replace r_m^* with the average mixing ratio at the same vertical level in the 100th percentile column r_{100}.

$$\Delta T = T\left(\frac{1+{r_{100}}/{\epsilon}}{1+r_{100}} - \frac{1+{r}/{\epsilon}}{1+r}\right)\left(\frac{1+r_{100}}{1+{r_{100}}/{\epsilon}}\right) \qquad [S8]$$

Since r_{100} is known, we do not need to use an iterative method to calculate ΔT. However, this calculation requires a relatively complete knowledge of the atmosphere, which is often lacking in the real world. Figure S7 shows this calculation of ΔT, which compares well with results in Fig. 6.

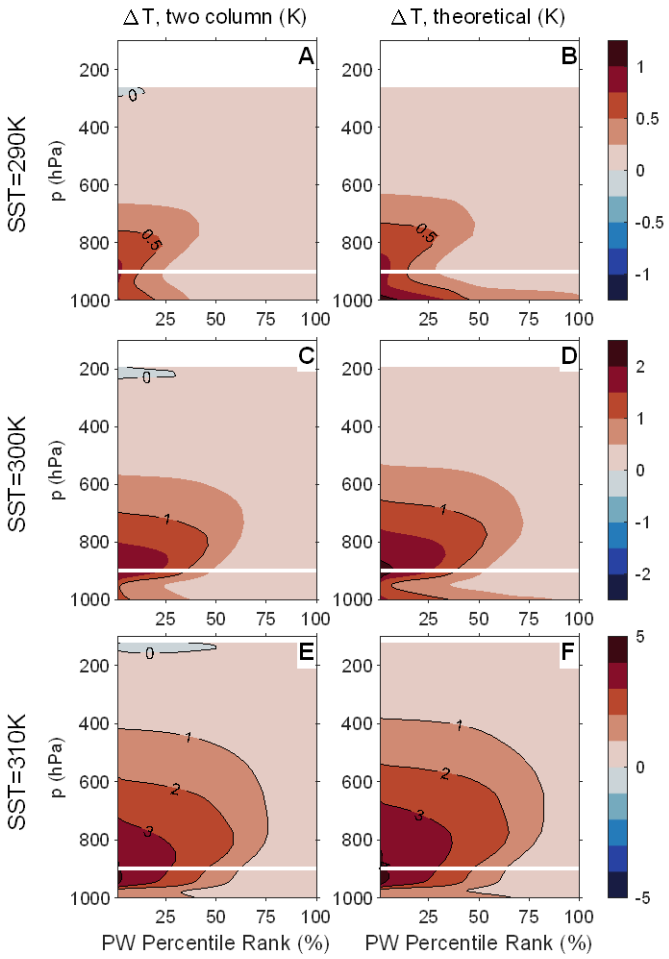

Figure S7. Alternate calculation of ΔT. (A, C, E) An alternate calculation of ΔT which is calculated by assuming every air parcel the same density as that of the 100th percentile rank column. **(B, D, F)** A duplication of the theory-based calculation of ΔT which was presented in Fig. 6. We do not show values of ΔT above the tropopause, where WBG no longer applies.